Liu C. M. (Orcid ID: 0000-0002-9705-5387)

Graham D. B. (Orcid ID: 0000-0002-1046-746X)

Khotyaintsev Yu. V. (Orcid ID: 0000-0001-5550-3113)

Fu H. S. (Orcid ID: 0000-0002-4701-7219)

Johlander A. (Orcid ID: 0000-0001-7714-1870)

André M. (Orcid ID: 0000-0003-3725-4920)

Giles B. L. (Orcid ID: 0000-0001-8054-825X)

Ion-beam-driven intense electrostatic solitary waves in reconnection jet

C. M. Liu[1,2], A. Vaivads[2,3], D. B. Graham[2], Yu. V. Khotyaintsev[2], H. S. Fu[1†], A. Johlander[2,4,5], M. André[2], and B. L. Giles[6]

[1]School of Space and Environment, Beihang University, Beijing, China

[2]Swedish Institute of Space Physics, Uppsala, Sweden

[3]Space and Plasma Physics, School of Electrical Engineering and Computer Science, KTH Royal Institute of Technology, Stockholm, Sweden

[4]Department of Physics and Astronomy, Uppsala University, Uppsala, Sweden

[5]Department of Physics, University of Helsinki, Helsinki, Finland

[6]NASA Goddard Space Flight Center, Greenbelt, Maryland, USA

This article has been accepted for publication and undergone full peer review but has not been through the copyediting, typesetting, pagination and proofreading process which may lead to differences between this version and the Version of Record. Please cite this article as doi: 10.1029/2019GL085419

†Correspondence to H. S. Fu at huishanf@gmail.com

Key points:

- Source and role of intense ESWs in a reconnection jet are investigated with MMS data
- Accelerated cold ion beams in the jet are found to be the source of the waves
- Wave-beam interaction can provide a new channel for particle heating in the jet

Abstract. Electrostatic solitary waves (ESWs) have been reported inside reconnection jets, but their source and role remain unclear hitherto. Here we present the first observational evidence of ESWs generation by cold ion beams inside the jet, by using high-cadence measurements from the Magnetospheric Multiscale spacecraft in the Earth's magnetotail. Inside the jet, intense ESWs with amplitude up to 30 mV m^{-1} and potential up to ~7% of the electron temperature, are observed in association with accelerated cold ion beams. Instability analysis shows that the ion beams are unstable, providing free energy for the ESWs. The waves are observed to thermalize the beams, thus providing a new channel for ion heating inside the jet. Our study suggests that electrostatic turbulence can play an important role in the jet dynamics.

1. Introduction

Magnetic reconnection is a fundamental plasma process, during which magnetic energy is converted into particle thermal and kinetic energy via reconfiguration of the magnetic topology (*Yamada et al*., 2010; *Fu et al*., 2017). Energy budgets between magnetic energy, particle kinetic energy, and thermal energy in magnetic reconnection have been well studied by numerical simulations (*Birn & Hesse.* 2010, 2014; *Lu et al.*, 2013, 2018). Reconnection

plays an important role in many explosive phenomena in the universe, such as stellar flares, coronal mass ejection, gamma-ray bursts, and substorms in the terrestrial magnetotail (*Angelopoulos et al*., 2008). During reconnection processes, the initially separated plasmas become magnetically connected, and the connected plasmas get ejected from reconnection region, producing high-speed plasma flows, commonly referred to as reconnection jets or burst bulk flows (BBFs) (*Angelopoulos et al*., 1992; *Cao et al.*, 2006, 2013). Reconnection jets have been suggested to be responsible for energy dissipation, particle heating and acceleration in space plasmas (e.g., *Khotyaintsev et al*., 2011; *Fu et al*., 2011; *Lapenta et al*., 2014; *Lu et al*., 2016; *Zhou et al*., 2018; *Sitnov et al*., 2019; *Chen et al.*, 2019; *Zhao et al.*, 2019).

Reconnection jet dynamics is closely related to their interaction with the ambient plasmas. Such interaction leads to formation of particle beams (*Wygant et al*., 2005; *Aunai et al*., 2011; *Eastwood et al*., 2015), rearrangement of the local current system (*Lu et al*., 2016), and various types of kinetic-scale instabilities developing inside the jets, such as anisotropy instability (*Khotyaintsev et al*., 2011; *Huang et al*., 2012; *Fu et al*., 2014; *Liu et al*., 2017a), streaming instability (*Deng et al*., 2010; *Yang et al*., 2017), kinetic ballooning or interchange instability (*Pritchett et al*., 2014, 2018; *Nakamura et al*., 2016) and lower hybrid drift instability at the jet front/dipolarization front (*Khotyaintsev et al*., 2011; *Divin et al*., 2015; *Liu et al*., 2018a, 2018b; *Pan et al*., 2018). These instabilities can generate strong electrostatic/electromagnetic waves that may interact with the local plasmas, leading to energy dissipation and particle heating (*Khotyaintsev et al*., 2011, 2017; *Huang et al*., 2014; *Huang et al*., 2015; *Fu et al*., 2012a; *Liu et al*., 2017b, 2017c; *Yao et al*., 2017; *Chen et al*., 2019). However, the wave generation and the associated wave-particle interaction have been difficult to diagnose from spacecraft measurements due to the involved small spatiotemporal

scales (e.g., electron scale or Debye scale) before the advent of the Magnetospheric Multiscale mission (MMS) (*Burch et al.*, 2015).

In particular, one type of nonlinear electrostatic structure characterized by bipolar change of parallel electric fields at Debye scale, traditionally referred to as electrostatic solitary waves (ESWs), electron holes or time domain structure (*Mozer et al.*, 2015), has been recently reported inside the jets (e.g., *Deng et al*., 2010; *Ergun et al*., 2014a). ESWs have also been frequently observed in reconnection region, such as at separatrix and inside magnetic flux ropes (*Khotyaintsev et al*., 2010; *Wang et al*., 2014; *Huang et al*., 2014), with distinct speeds reported (*Graham et al*., 2015): fast ESWs with speeds close to electron thermal speed are suggested to be driven by high-speed electron beam (e.g., *Omura et al*., 1996; *Drake et al*., 2003; *Che et al*., 2009), while slow ESWs with speeds close to ion thermal speed are suggested to be generated by Buneman instability (*Khotyaintsev et al*., 2010; *Norgren et al*. 2015). However, for ESWs inside the jets, their properties (e.g., speed and potential) and generation mechanisms, remain unclear so far.

In this study, we use high-cadence measurements of a reconnection jet by the MMS spacecraft to study the interactions between ESWs and particle beams inside a reconnection jet in the Earth's magnetotail. We present the first observational evidence of ESWs generation by accelerated cold ion beams inside the jet and investigate their properties and role in the jet dynamics.

2. Observations

The magnetic field data from the fluxgate magnetometer (*Russell et al.*, 2014), electric field data from the electric field double probes (*Lindqvist et al*., 2014; *Ergun et al*., 2014b), and particle data from the fast plasma investigation (*Pollock et al*., 2016) are used. A typical event with intense ESWs observed inside the reconnection jet is studied, as shown in Figure 1.

All data are presented in **NML** coordinates, which are derived from the minimum variance analysis of **B** during the jet front crossing, unless otherwise specified. Here **L** is approximately parallel to **B**, **N** is normal to the jet front, and **M** completes the right handed **NML** system. Relative to GSM coordinates, the local coordinates are: **L**=[0.14, -0.64, 0.76], **N**=[0.92, 0.36, 0.13], and **M**=[-0.36, 0.68, 0.64].

The jet front (JF), also usually referred to as dipolarization front (*Nakamura et al*., 2002; *Runov et al*., 2009; *Fu et al*., 2012b), is characterized by the rapid increase of B_L (Figure 1a), decrease of electron density (Figure 1b), and intense electric fields therein (Figures 1c and 1d). The strong-B region behind the JF is traditionally referred to as flux pileup region (FPR) (*Khotyaintsev et al*., 2011; *Fu et al*., 2013a) or dipolarizing flux bundle (DFB) (*Liu et al*., 2013). The JF is observed by all of the MMS spacecraft, and timing analysis yields its propagation velocity $\boldsymbol{V}_{JF}$ = 1530*(0.96, 0.28, 0.08) km s^{-1} in GSM coordinates, close to the local Alfvén speed. JF is usually considered as a consequence of magnetic reconnection in the mid tail (*Fu et al*., 2013b; *Xu et al*., 2018a). The JF propagation direction derived from the timing analysis is almost same as the normal direction obtained from the MVA analysis. The reconnection jet has a maximum velocity approaching 1200 km/s (note that the jet speed may be underestimated because FPI may not capture the whole ion distribution) (see Figure 1e), ~0.8 $V_{Alfvén}$ ($V_{Alfvén}$ is the local Alfvén speed). The JF thickness (defined as the distance between B_L minimum and maximum) is estimated as 600 km, ~1.2 d_i, where $d_i = c/\omega_{pi}$ is the ion inertial length calculated based on the density prior to the JF arrival. The intense electric fields at the JF, with both N and M components dominant (Figure 1c), exhibit spiky features. Such features are due to the ripples generated by lower hybrid drift instability, which is driven by density gradient at the front (*Liu et al*., 2018b; *Pan et al*., 2018). Sharp changes in the electron and ion distributions are observed at the JF crossing. Figure 1f shows electron 1D reduced distribution function in the direction parallel to **B** and Figure 1g displays ion 1D

reduced distribution function in the **L** direction. Across the front, electrons become hotter and more dilute, and there is no field-aligned beams (Figure 1f). The ion distribution changes from nearly flat-top distribution to clearly counter-streaming distribution (Figure 1g). The sharp changes are also clear in the ion and electron energy spectrogram (Figures 1h and 1i), in which we see that the electrons get heated and accelerated inside the flux pileup region (*Fu et al*., 2019a, 2019b; *Birn et al*., 2013; *Liu et al*., 2019; *Xu et al*., 2018b).

Now we focus on the flux pileup region behind the JF, where large-amplitude E_M and E_L components are observed. The persistent $E_M \sim V_N \times B_L$ is the motional electric field arising from the enhanced magnetic field strength and high-speed flow (*Fu et al.,* 2012c; *Liu et al*., 2018b). The short-period intense $E_L \sim E_{\parallel}$ is the parallel electric field as the angle between the **L** direction and the local **B** is less than 3 degrees. The localized $E_{\parallel}$ exhibits asymmetrically bipolar features and has broadband power spectrogram (not shown), and thus they are interpreted as electrostatic solitary waves (ESWs) (*Deng et al*., 2010; *Graham et al.*, 2015, 2016). Associated with the intense ESWs, no clear electron-beam signature is observed (Figure 1f), indicating that they are not related to the instabilities involving electrons, such as electron beam instability or Buneman instability; instead, we find two counter-streaming cold ion beams in the field-aligned direction (Figure 1g). This suggests that the ESWs may be generated by the ion beams.

To reveal the wave properties and wave-beam interactions in detail, we present four spacecraft observations of the ESWs and the associated ion 2D reduced velocity distributions in Figure 2. Figures 2a and 2b show B_L and currents calculated by the curlometer method. During observations of the ESWs, the magnetic field decreases gradually and the local currents are very weak, indicating that the ESWs are not associated with strong currents. The ESWs are observed by all four MMS spacecraft (Figure 2c), and the waves observed by different spacecraft are almost the same when we compare the time-shifted fields of the four

spacecraft (Figure 2d), such that we can resolve the wave speed unambiguously (*Steinvall et al*., 2019). Using timing analysis, we calculate the wave propagation velocity to be $\boldsymbol{V}_{\mathrm{ESWs}}$ = 820*[-0.06, 0.60, 0.79] km s^{-1}, which is comparable to the local ion thermal speed and antiparallel to the local magnetic field. Considering the propagation velocity and polarity of the ESWs, we find that the electric field is diverging, and thus the ESWs correspond to electron holes rather than ion holes. Based on the wave speed and wave period, we estimate the wave peak-peak length scale as $I_{pp} \approx 9.5\,\lambda_D$, where λ_D is the local Debye length. The length scale of the observed ESWs is comparable to those observed at the Earth's magnetopause (*Graham et al*., 2016). Using the resolved wave speed, we calculate the wave electrostatic potential via integration of $E_{\parallel}$: $\phi = -\int E_{\parallel}\ V_{ESWs}dt$ (Figure 2e). We see that the ESWs have potential humps of 50-120 V, and contain a peak potential of ~200 V, which corresponds to ~7% of the electron thermal temperature.

Figures 2f-2h show the ion 2D reduced distribution in the **L-N** plane. We can see that two cold ion beams are clearly observed along with the ESWs. The two cold beams have similar speed in the **N** direction, which is close to jet speed, but propagate in opposite directions along **L** (or field-aligned direction). The counter-streaming cold ion beams have a maximum relative drift speed approaching 2000 km s^{-1}. We observe evidence of beam-wave interaction, which is manifested in the short-time local evolution of the ion distribution during the wave interval: cold ion beams are first seen before the waves, then the beams become rapidly thermalized within the waves, and get thermalized further after the waves. Note that considering the wave speed and potential, the waves can trap ions with speeds between $V_T = V_{ph} \pm \sqrt{2q_e\Phi/m_i} \approx [-820 \pm 150]$ km s^{-1}, which mainly lies on the ion population propagating in the **-L** direction. This means that only the ion beam propagating in the same direction as the waves would be heated, consistent with the observations. Due to the absence of electron beams or strong currents, the cold ion beams are the most probable source

of the ESWs (note that the asymmetric feature and varying amplitude of the ESWs indicate that the waves are still in the evolution phase; as such, their source should be nearby). Therefore, we conclude that the ESWs may be driven by ion beam instability.

3. Instability analysis

To investigate the instability associated with these cold ion beams propagating along the magnetic field line, we consider a plasma containing four ion population (both hydrogen and oxygen) and one electron population. Here we assume that the electrons have zero drift. Under these assumptions, the electrostatic dispersion relation is:

$$1-\frac{\omega_{pih1}^2}{k^2V_{ih1}^2}Z'\left(\frac{\omega-kV_{ihb1}}{kV_{ih1}}\right)-\frac{\omega_{pih2}^2}{k^2V_{ih2}^2}Z'\left(\frac{\omega-kV_{ihb2}}{kV_{ih2}}\right)-\frac{\omega_{pio1}^2}{k^2V_{io1}^2}Z'\left(\frac{\omega-kV_{iob1}}{kV_{io1}}\right)-$$

$$\frac{\omega_{pio2}^2}{k^2V_{io2}^2}Z'\left(\frac{\omega-kV_{iob2}}{kV_{io2}}\right)-\frac{\omega_{pe}^2}{k^2V_e^2}Z'\left(\frac{\omega}{kV_e}\right)=0, \quad (1)$$

where the subscripts $i_{ih1,ih2,io1,io2}$ refer to the hydrogen and oxygen beams, $\omega_{px}=\sqrt{n_x q_e^2/m_x\epsilon_0}$ ($x=ih1,ih2,io1,io2,e$) are the ion and electron plasma frequencies, Z' is the derivative of the plasma dispersion function, $V_{ih1,ih2,io1,io2}$ are the ion beam velocities, $v_{ih1,ih2,io1,io2,e}$ are the ion and electron thermal speeds. Here the oxygen population is considered due to following reasons: I. In the initial analysis, when we consider hydrogen only, beams are found to be unstable but the predicted phase speed is about three times slower than observed wave speed, suggesting possible importance of heavier ions; II. When we include oxygen beams, beams are still unstable but the prediction becomes closer to the observation; and if we consider only oxygen, the prediction well matches the observation, indicating that oxygen can indeed play a crucial role; III. In the adjacent lobe region, the inflow region to the reconnection site, we observe that both oxygen and hydrogen are dominant and have comparable density (not shown), strongly suggesting that oxygen can be dominant in the reconnection jet as well; however, very few heavier ions are observed inside the jet by HPCA instrument which measures ions up to 40 keV at a 10s cadence, and the reason, is that most of oxygen is at high energies—>80 keV, estimated based on Fermi acceleration of oxygen;

presence of energetic ions is observed by EIS instrument which measures energetic ions up to 500 keV; but the count statistics is not good enough to reconstruct the distribution function of oxygen and therefore for the instability analysis we base the oxygen distribution function on assumption that oxygen has experienced the same Fermi acceleration process as hydrogen (see discussions below). Here we assume that oxygen beam has same speed as hydrogen beam because Fermi acceleration is independent of ion mass.

To obtain the beam parameters for solving equation (1), we fit the 1D ion reduced distribution along **L** observed before the waves, by using two Maxwellian distributions (Figure 3a). The beam parameters obtained from the fitting are $n_{ib1} = 0.026$ cm^{-3}, $T_{ib1} = 300$ eV, $V_{ib1} = -900$ km s^{-1}, $n_{ib2} = 0.009$ cm^{-3}, $T_{ib2} = 200$ eV, and $V_{ib2} = 950$ km s^{-1}. With these parameters, the predicted properties of the unstable beam mode are obtained in Figure 3b. We see that the ion beams are indeed unstable, and the wave number with positive growth rate ranges from 0 to 2.1 × 10^{-4} m^{-1}. The wave number of the observed ESWs, $k_{ESWs} \sim 1.5 \times 10^{-4}$ m^{-1}, falls well inside this range. Moreover, the predicted wave speed corresponding to the observed wave number k_{ESWs} is ~400 km s^{-1}, close to the observed ESWs. In addition, the beam energy density, $W_{b1} = m_i n_{b1} v_{b1}^2/2 \sim 2.4 \times 10^{-12}$J m^{-3}, is much larger than the maximum wave field energy density, $W_E = \varepsilon_0 |E|^2/2 \sim 4 \times 10^{-15}$ J m^{-3}, consistent with the cold ion beams providing free energy for the waves. And the thermalized ion beams observed behind the waves are found to be stable (showing negative growth rate, not shown). These calculations suggest that the ESWs are driven by the ion beam instability. We notice that the predicted wave speed is slower than the observed speed, indicating that the observed beams or waves may have been affected by other momentum-exchange processes, such as ion drag introduced by the waves. The asymmetrically bipolar feature of the ESWs indicates that the electrostatic structures are still experiencing temporal evolution which may also have changed the wave properties (*Wu et al.*, 2010). Note that

uncertainties arising from the fitting of ion distribution function and the assumption about oxygen parameters in the analysis may contribute to the difference between observations and predictions as well.

4. Discussion and Summary

Generation mechanisms for the intense ESWs observed inside the jet are different from those observed in the reconnection region, such as fast ESWs at separatrix and slow ESWs inside the flux rope, which are associated with fast electron beam or strong currents (e.g. *Drake et al*., 2003; *Che et al*., 2009; *Khotyaintsev et al*., 2010; *Wang et al*., 2014). The intense ESWs observed inside the jet are not associate with electron beam or strong currents; instead, they are driven by fast cold ion beams which are formed during jet propagating away from the reconnection region.

Two physical mechanisms may account for accelerated ion beams observed inside the jet. One mechanism is connected with the interactions between the earthward propagating flux tubes and the ambient plasma: ambient cold ions is accelerated due to Fermi acceleration when they encounter the bent flux tubes (*Eastwood et al*., 2015; *Xu et al*., 2019). Such mechanism should dominate in our case, because the observed beam speed is close to the jet speed in neutral sheet, as predicted by Fermi mechanism. Based on this, assuming oxygen beam speed same as hydrogen beam speed in the instability analysis is reasonable because Fermi acceleration is independent of ion mass. Such assumption may be not exactly accurate due to potential role of the other mechanism that the cold ions are accelerated by potential jump across the separatrix (*Wygant et al*., 2005). In Figure 4 we schematically illustrate the trajectories of the accelerated ion beams and the excitation of the ESWs inside the reconnection jet. Accelerated ion beams that are formed in the jet can be unstable to ion beam instability and drive electrostatic waves which move along the magnetic field line at slow speeds. Due to the propagation of the waves and beams, or the instability conditions, the

waves and beams may not exhibit nice one-to-one correlation, as is the case in our observations. The waves can lead to local ion heating, in addition to the mirror or firehose instabilities reported in previous studies (*Wu et al.*, 2013).

In summary, using high-cadence measurements from jet crossing by the Magnetospheric Multiscale (MMS) spacecraft, we present the first observational evidence of ESWs generation by accelerated cold ion beams inside the reconnection jet. The accelerated ion beams are formed during the jet propagating away from the reconnection region and unstable to ion beam instability, which drives the intense ESWs with potential up to ~7% of the electron temperature. The ESWs conversely thermalize the cold ion beams, thus providing an new channel for particle heating inside jets. Our observations suggest that ESWs can play an important role in jet dynamics.

Acknowledgments. We thank the MMS Science Data Center (https://lasp.colorada.edu/mms/sdc/public/) for providing the excellent data for this study. This work is supported by NSFC grants 41404133, 41874188, 41574153, 40621003, and 41431071. C. M. Liu is supported by the Academic Excellence Foundation of BUAA for PhD Students and the scholarship from the Chinese Scholarship Council.

References

Angelopoulos, V., W. Baumjohann, C. F. Kennel, F. V. Coroniti, M. G. Kivelson, R. Pellat, R. J. Walker, H. Lühr, and G. Paschmann (1992), Bursty bulk flows in the inner central plasma sheet, *J. Geophys. Res.*, *97*(A4), 4027–4039, doi:10.1029/91JA02701.

Angelopoulos, V., et al. (2008), Tail reconnection triggering substorm onset, *Science*, 321, 931–935

Aunai, N., Belmont, G., and Smets, R (2011) Proton acceleration in antiparallel collisionless magnetic reconnection: Kinetic mechanisms behind the fluid dynamics, *J. Geophys. Res. Space Physics, 116,* A09232,, doi: 10.1029/2011JA016688

Birn, J., & Hesse, M (2010). Energy release and transfer in guide field reconnection. *Physics of Plasmas, 17(1),* 012109. https://doi.org/10.1063/1.3299388

Birn, J., M. Hesse, R. Nakamura, and S. Zaharia (2013), Particle acceleration in dipolarization events, *J. Geophys. Res. Space Physics, 118*, 1960–1971, doi:10.1002/jgra.50132

Birn, J., and M. Hesse (2014), Forced reconnection in the near magnetotail: Onset and energy conversion in PIC and MHD simulations. J Geophys. Res. Space Physics,119,290–309, doi:10.1002/2013JA019354

Burch, J. L., T. E. Moore, R. B. Torbert, and B. L. Giles (2015), Magnetospheric multiscale overview and science objectives, *Space Sci. Rev., 199*, 5–21, doi:10.1007/s11214-015-0164-9

Cao, J. B., et al. (2006), Joint observations by Cluster satellites of bursty bulk flows in the magnetotail, *J. Geophys. Res., 111*, A04206, doi:10.1029/2005JA011322

Cao, J., Ma, Y., Parks, G., Reme, H., Dandouras, I., & Zhang, T. (2013). Kinetic analysis of the energy transport of bursty bulk flows in the plasma sheet. *Journal of Geophysical Research: Space Physics, 118*, 313–320. https://doi.org/10.1029/2012JA018351

Che, H., Drake, J. F., Swisdak, M., & Yoon, P. H. (2010). Electron holes and heating in the reconnection dissipation region. *Geophysical Research Letters, 37*, L11105. https://doi.org/10.1029/2010GL043608

Chen, Z. Z., Fu, H. S., Liu, C. M., Wang, T. Y., Ergun, R. E., Cozzani, G., et al. (2019). Electron-driven dissipation in a tailward flow burst. *Geophysical Research Letters, 46*, 5698–5706. https://doi.org/10.1029/2019GL082503

Chen, G., et al. (2019). Energetic Electron Acceleration in Unconfined Reconnection Jets. *Astrophysical Journal Letters, 881(1),* L8. https://doi.org/10.3847/2041-8213/ab3041

Deng, X., M. Ashour-Abdalla, M. Zhou, R. Walker, M. El-Alaoui, V. Angelopoulos, R. E. Ergun, and D. Schriver (2010), Wave and particle characteristics of earthward electron injections associated with dipolarization fronts, *J. Geophys. Res., 115*, A09225, doi:10.1029/2009JA015107

Divin, A., Y. V. Khotyaintsev, A. Vaivads, and M. André (2015), Lower hybrid drift instability at a dipolarization front, *J. Geophys. Res. Space Physics, 120*, 1124–1132, doi:10.1002/2014JA020528

Drake, J. F., Swisdak, M., Cattell, C., Shay, M. A., Rogers, B. N., & Zeiler, A. (2003). Formation of electron holes and particle energization during magnetic reconnection. *Science, 5608*, 873–877. https://doi.org/10.1126/science.1080333

Eastwood, J. P., Goldman, M. V., Hietala, H., Newman, D. L., Mistry, R., & Lapenta, G. (2015). Ion reflection and acceleration near magnetotail dipolarization fronts associated with magnetic reconnection. *Journal of Geophysical Research: Space Physics, 120*, 511–525. https://doi.org/10.1002/2014JA020516

Ergun, R. E., et al. (2014), The Axial Double Probe and Fields Signal Processing for the MMS Mission, *Space Sci. Rev., 199*, 167–188,doi:10.1007/s11214-014-0115-x

Ergun, R. E., Goodrich, K. A., Stawarz, J. E., Andersson, L., & Angelopoulos, V. (2014). Large-amplitude electric fields associated with bursty bulk flow braking in the Earth's plasma sheet. *Journal of Geophysical Research: Space Physics, 120*, 1832–1844. https://doi.org/10.1002/2014JA020165

Fu, H. S., Y. V. Khotyaintsev, M. André, and A. Vaivads (2011), Fermi and betatron acceleration of suprathermal electrons behind dipolarization fronts, *Geophys. Res. Lett., 38*, L16104, doi:10.1029/2011GL048528.

Fu, H. S., Y. V. Khotyaintsev, A. Vaivads, M. André, V. A. Sergeev, S. Y. Huang, E. A. Kronberg, and P. W. Daly (2012a), Pitch angle distribution of suprathermal electrons behind dipolarization fronts: A statistical overview, *J. Geophys. Res., 117*, A12221, doi:10.1029/2012JA018141

Fu, H. S., Y. V. Khotyaintsev, A. Vaivads, M. André, and S. Y. Huang (2012b), Occurrence rate of earthward-propagating dipolarization fronts, *Geophys. Res. Lett.*, *39*, L10101, doi:10.1029/2012GL051784

Fu, H. S., Y. V. Khotyaintsev, A. Vaivads, M. André, and S. Y. Huang (2012c), Electric structure of dipolarization front at sub-proton scale, *Geophys. Res. Lett.*, 39, L06105, doi:10.1029/2012GL051274

Fu, H. S., Y. V. Khotyaintsev, A. Vaivads, A. Retinò, and M. André (2013a), Energetic electron acceleration by unsteady magnetic reconnection, *Nat. Phys.*, *9*, 426–430, doi:10.1038/NPHYS2664

Fu, H. S., et al. (2013b), Dipolarization fronts as a consequence of transient reconnection: In situ evidence, *Geophys. Res. Lett.*, 40, 6023–6027, doi:10.1002/2013GL058620

Fu, H. S., et al. (2014), Whistler-mode waves inside flux pileup region: Structured or unstructured?, *J. Geophys. Res. Space Physics*, *119*, 9089–9100, doi:10.1002/2014JA020204

Fu, H. S., Vaivads, A., Khotyaintsev, Y. V., André, M., Cao, J. B., Olshevsky, V., et al. (2017). Intermittent energy dissipation by turbulent reconnection. *Geophysical Research Letters*, *44*, 37–43. https://doi.org/10.1002/2016GL071787

Fu, H. S., Xu, Y., Vaivads, A., & Khotyaintsev, Y. V. (2019a). Super-efficient electron acceleration by an isolated magnetic reconnection. *Astrophysical Journal Letters*, *870(2)*, L22. https://doi.org/10.3847/2041-8213/aafa75

Fu, H. S., Peng, F. Z., Liu, C. M., Burch, J. L., Gershman, D. J., O. Le Contel (2019b). Evidence of Electron Acceleration at a Reconnecting Magnetopause. *Geophysical Research Letters*, *44*, 37–43. https://doi.org/10.1002/2016GL071787

Graham, D. B., Khotyaintsev, Y. V., Vaivads, A., & André, M. (2015). Electrostatic solitary waves with distinct speeds associated with asymmetric reconnection. *Geophysical Research Letters*, *42*, 215–224. https://doi.org/10.1002/2014GL062538

Graham, D. B., Khotyaintsev, Y. V., Vaivads, A., & André, M. (2016). Electrostatic solitary waves and electrostatic waves at the magnetopause. *Journal of Geophysical Research: Space Physics, 121,* 3069–3092. https://doi.org/10.1002/2015JA021527

Huang, C., Q. Lu, P. Wang, M. Wu, and S. Wang (2014), Characteristics of electron holes generated in the separatrix region during antiparallel magnetic reconnection, *J. Geophys. Res. Space Physics, 119,* 6445–6454, doi:10.1002/2014JA019991.

Huang, S. Y., M. Zhou, X. H. Deng, Z. G. Yuan, Y. Pang, Q. Wei, W. Su, H. M. Li, and Q. Q. Wang (2012), Kinetic structure and wave properties associated with sharp dipolarization front observed by Cluster, *Ann. Geophys., 30,* 97–107, doi:10.5194/angeo-30-97-2012

Huang, S. Y., et al. (2015), Electromagnetic energy conversion at dipolarization fronts: Multispacecraft results, *J. Geophys. Res. Space Physics, 120,* 4496–4502, doi:10.1002/2015JA021083

Hwang, K.-J., M. L. Goldstein, A. F.-Vinas, D. Schriver, and M. Ashour-Abdalla (2014), Wave-particle interactions during a dipolarization front event, *J. Geophys. Res. Space Physics, 119,* 2484–2493, doi:10.1002/2013JA019259

Khotyaintsev, Y. V., Vaivads, A., André, M., Fujimoto, M., Retinò, A., & Owen, C. (2010). Observations of slow electron holes at a magnetic reconnection site. *Physical Review Letters, 105(16),* 165002. https://doi.org/10.1103/PhysRevLett.105.165002

Khotyaintsev, Y. V., C. M. Cully, A. Vaivads, M. André, and C. J. Owen (2011), Plasma jet braking: energy dissipation and nonadiabatic electrons, *Physical Review Letters, 106,* 165001. doi:10.1103/PhysRevLett.106.165001

Khotyaintsev, Y. V., A. Divin, A. Vaivads, M. André, and S. Markidis (2017), Energy conversion at dipolarization fronts, *Geophys. Res. Lett., 44,* 1234-1242. doi:10.1002/2016GL071909

Lapenta, G., M. Goldman, D. Newman, S. Markidis, and A. Divin (2014), Electromagnetic energy conversion in downstream fronts from three dimensional kinetic reconnection, *Phys. Plasmas, 21(5)*, 055702, doi:10.1063/1.4872028

Lindqvist, P.-A., et al. (2014), The spin-plane double probe electric field instrument for MMS, *Space Sci. Rev., 199*, 137–165, doi:10.1007/s11214-014-0116-9

Liu, J., V. Angelopoulos, X.-Z. Zhou, A. Runov, and Z. H. Yao (2013), On the role of pressure and flow perturbations around dipolarizing flux bundles, *J. Geophys. Res. Space Physics, 118*, 7104-7118, doi:10.1002/2013JA019256

Liu, C. M., H. S. Fu, Y. Xu, T. Y. Wang, J. B. Cao, X. G. Sun, and Z. H. Yao (2017a), Suprathermal electron acceleration in the near-earth flow rebounce region, *J. Geophys. Res. Space Physics, 122*, 594–604. doi:10.1002/2016JA023437

Liu, C. M., H. S. Fu, Y. Xu, J. B. Cao, and W. L. Liu (2017b), Explaining the rolling-pin distribution of suprathermal electrons behind dipolarization fronts, *Geophys. Res. Lett., 44*, 6492–6499. doi:10.1002/2017GL074029

Liu, C. M., Fu, H. S., Cao, J. B., Xu, Y., Yu, Y. Q., Kronberg, E. A., & Daly, P. W. (2017c). Rapid pitch angle evolution of suprathermal electrons behind dipolarization fronts. *Geophysical Research Letters, 44*. 10116–10124. https://doi.org/10.1002/2017GL075007

Liu, C. M. et al (2018a). Electron jet detected by MMS at dipolarization front. *Geophysical Research Letters, 45*. 556–564. https://doi.org/10.1002/2017GL076509

Liu, C. M., Fu, H. S., Xu, Y., Khotyaintsev, Y. V., Burch, J. L., Ergun, R. E., et al. (2018b). Electron-scale measurements of dipolarization front. *Geophysical Research Letters, 45*, 4628–4638. https://doi.org/10.1029/2018GL077928

Liu, C. M., & Fu, H. S. (2019). Anchor point of electron acceleration around dipolarization fronts in space plasmas. *Astrophysical Journal Letters, 873(1)*, L2. https://doi.org/10.3847/2041-8213/ab06cb

Lu, S., Lu, Q. M., Huang, C., & Wang, S. (2013). The transfer between electron bulk kinetic energy and thermal energy in collisionless magnetic reconnection. *Physics of Plasmas, 20(6)*, 061203. https://doi.org/10.1063/1.4811119

Lu, S., Artemyev, A. V., Angelopoulos, V., Lu, Q., & Liu, J. (2016). On the current density reduction ahead of dipolarization fronts. *Journal of Geophysical Research: Space Physics, 121*, 4269–4278. https://doi.org/10.1002/2016JA022754

Lu, S., V. Angelopoulos, H. S. Fu (2016), Suprathermal particle energization in dipolarization fronts: Particle-in-cell simulations, *J. Geophys. Res. Space Physics*, 121, doi:10.1002/2016JA022815

Lu, S., Pritchett, P. L., Angelopoulos, V., & Artemyev, A. V. (2018). Magnetic reconnection in Earth's magnetotail: Energy conversion and its earthward-tailward asymmetry. *Physics of Plasmas, 25(1)*, 012905. https://doi.org/10.1063/1.5016435

Mozer, F. S., Agapitov, O. V., Artemyev, A., Drake, J. F., Krasnoselskikh, V., Lejosne, S., & Vasko, I. (2015). Time domain structures: What and where they are, what they do, and how they are made. *Geophysical Research Letters, 42,* 3627–3638. https://doi.org/10.1002/2015GL063946

Nakamura, T. K. M., R. Nakamura, W. Baumjohann, T. Umeda, and I. Shinohara (2016), Three-dimensional development of front region of plasma jets generated by magnetic reconnection, *Geophys. Res. Lett., 43*, 8356–8364, doi:10.1002/2016GL070215

Norgren, C., André, M., Vaivads, A., & Khotyaintsev, Y. V. (2015). Slow electron phase space holes: Magnetotail observations. *Geophysical Research Letters, 42*, 1654–1661. https://doi.org/10.1002/2015GL063218

Omura, Y., Matsumoto, H., Miyake, T., & Kojima, H. (1996). Electron beam instabilities as generation mechanism of electrostatic solitary waves in the magnetotail. *Journal of Geophysical Research, 101(A2)*, 2685–2697. https://doi.org/10.1029/95JA03145

Pan, D.-X., Khotyaintsev, Y. V., Graham, D. B., Vaivads, A., Zhou, X.-Z., André, M., et al. (2018). Rippled electron-scale structure of a dipolarization front. *Geophysical Research Letters, 45*, 12116-12124. https://doi.org/10.1029/2018GL080826

Pollock, C., et al. (2016), Fast plasma investigation for magnetospheric multiscale, *Space Sci. Rev., 199,* 331–406, doi:10.1007/s11214-016-0245-4

Pritchett, P. L., F. V. Coroniti, and Y. Nishimura (2014), The kinetic ballooning/interchange instability as a source of dipolarization fronts and auroral streamers, *J. Geophys. Res. Space Physics, 119,* 4723–4739. doi:10.1002/2014JA019890

Pritchett, P. L., & Lu, S. (2018). Externally driven onset of localized magnetic reconnection and disruption in a Magnetotail configuration. *Journal of Geophysical Research: Space Physics, 123,* 2787–2800. https://doi.org/10.1002/2017JA025094

Runov, A., V. Angelopoulos, M. I. Sitnov, V. A. Sergeev, J. Bonnell, J. P. McFadden, D. Larson, K. H. Glassmeier, and U. Auster (2009), THEMIS observations of an earthward-propagating dipolarization front, *Geophys. Res. Lett., 36,* L14106, doi:10.1029/2009GL038980

Russell, C. T., et al. (2014), The magnetospheric multiscale magnetometers, *Space Sci. Rev., 199*, 189–256, doi:10.1007/s11214-014-0057-3

Sitnov, M., et al., (2019) Explosive Magnetotail Activity, *Space Sci. Rev., 215, 31,* https://doi.org/10.1007/s11214-019-0599-5

Steinvall, K., Khotyaintsev, Y. V., Graham, D. B., Vaivads, A., Lindqvist, P.-A., Russell, C. T., & Burch, J. L. (2019). Multispacecraft analysis of electron holes. *Geophysical Research Letters, 46*, 55–63. https://doi.org/10.1029/2018GL080757

Xu, Y., Fu, H. S., Liu, C. M., & Wang, T. Y. (2018a). Electron acceleration by dipolarization fronts and magnetic reconnection: A quantitative comparison. *Astrophysical Journal, 853(1),* 11. https://doi.org/10.3847/1538‐4357/aa9f2f

Xu, Y., Fu, H. S., Norgren, C., Hwang, K. ‐ J., & Liu, C. M. (2018b). Formation of dipolarization fronts after current sheet thinning. *Physics of Plasmas, 25(7),* 072123. https://doi.org/10.1063/1.5030200

Xu, Y., Fu, H. S., Norgren, C., Toledo-Redondo, S., Liu, C. M., and Dong, X. C (2019). Ionospheric Cold Ions Detected by MMS Behind Dipolarization Fronts. *Geophysical Research Letters, 46,* 7883-7892. https:// doi.org/10.1029/2019GL083885

Wang, R. S., et al. (2014), Observation of double layer in the separatrix region during magnetic reconnection, Geophys. Res. Lett.,41, 4851–4858,doi:10.1002/2014GL061157

Wygant, J. R., et al., (2019) Cluster observations of an intense normal component of the electric field at a thin reconnecting current sheet in the tail and its role in the shock-like acceleration of the ion fluid into the separatrix region, *J. Geophys. Res. Space Physics, 110*, A09206, doi: 10.1029/2004JA010708

Wu, M., Lu, Q., Huang, C., and Wang, S. (2010), Transverse instability and perpendicular electric field in two dimensional electron phase-space holes, *J. Geophys. Res.*, *115*, A10245, doi:10.1029/2009JA015235.

Wu, M. Y., Volwerk, M., Lu, Q. M., Vörös, Z., Nakamura, R., and Zhang, T. L. (2013), The proton temperature anisotropy associated with bursty bulk flows in the magnetotail, *J. Geophys. Res. Space Physics, 118*, 4875–4883, doi:10.1002/jgra.50451.

Yamada, M., R. Kulsrud, and H. Ji (2010), Magnetic reconnection, *Rev. Mod. Phys.*, *82*, 603–664, doi:10.1103/RevModPhys.82.603

Yang, J, J. B. Cao, H. S. Fu, T. Y. Wang, W. L. Liu, and Z. H. Yao (2017), Broadband high-frequency waves detected at dipolarization fronts, *J. Geophys. Res. Space Physics*, *122*, doi:10.1002/2016JA023465

Yao, Z., et al. (2017), A direct examination of the dynamics of dipolarization fronts using MMS, *J. Geophys. Res. Space Physics, 122*, doi:10.1002/2016JA023401

Zhao, M. J., Fu, H. S., Liu, C. M., Chen, Z. Z., Xu, Y., Giles, B. L., & Burch, J. L. (2019). Energy range of electron rolling-pin distribution behind dipolarization front. *Geophysical Research Letters, 46*, 2390–2398. https://doi.org/10.1029/2019GL082100

Zhou, X.-Z., Runov, A., Angelopoulos, V., Artemyev, A. V., & Birn, J. (2018). On the acceleration and anisotropy of ions within magnetotail dipolarizing flux bundles. *Journal of Geophysical Research: Space Physics, 123*. https://doi.org/10.1002/2017JA024901

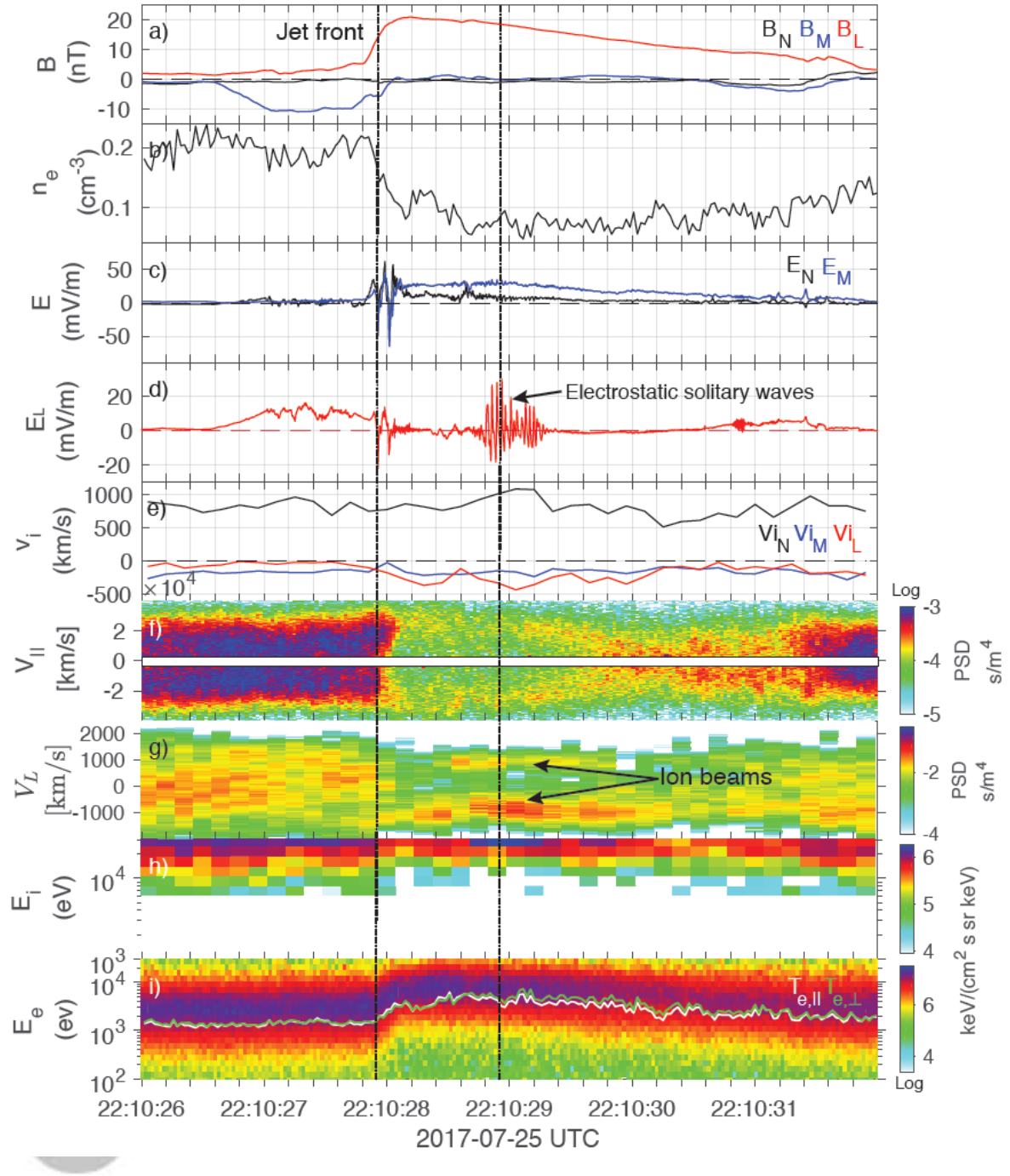

Figure 1. Jet crossing observed by MMS1. (a) magnetic field **B**. (b) electron density. (c) $\mathbf{E}_M$ and $\mathbf{E}_N$ components. (d) $\mathbf{E}_L$ component. (e) ion velocity. (f) electron phase space in the parallel direction (here electrons at energies <100 eV are excluded due to large uncertainty of electron measurements). (g) ion phase space in the **L** direction. (h) ion energy spectrum. (i) electron energy spectrum.

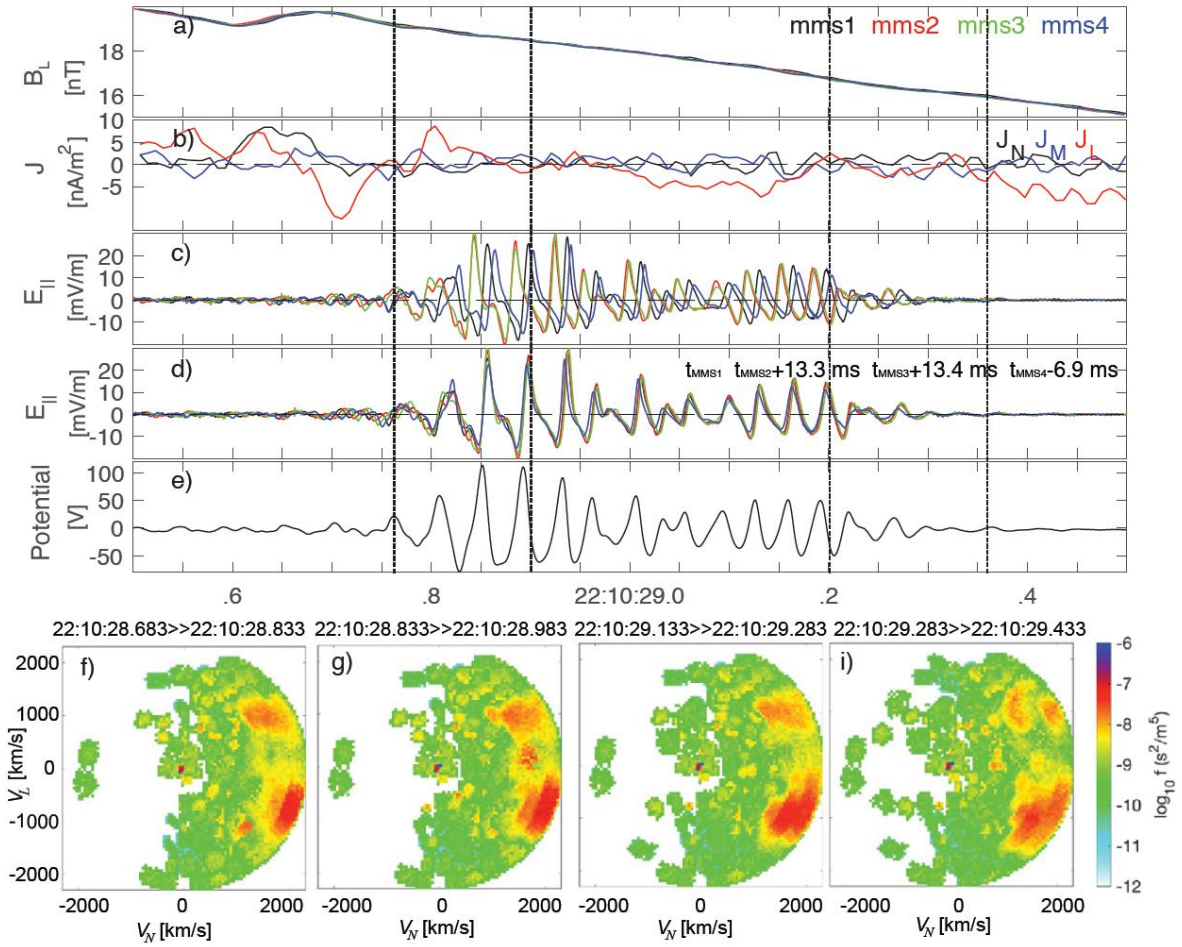

Figure 2. Four-spacecraft observations of the ESWs and ion distribution functions. (a) magnetic field $\mathbf{B}_L$ component. (b) currents calculated by curlometer method. (c) parallel electric fields. (d) time-shifted parallel electric fields. (e) wave potential. (f-h) ion distribution functions in the $\mathbf{V}_L$-$\mathbf{V}_N$ plane. MMS1-MMS4 data are shown in black, red, green and blue, respectively. The ion distribution is averaged over four spacecraft (here the nearest point in time among the spacecraft measurements is used for averaging).

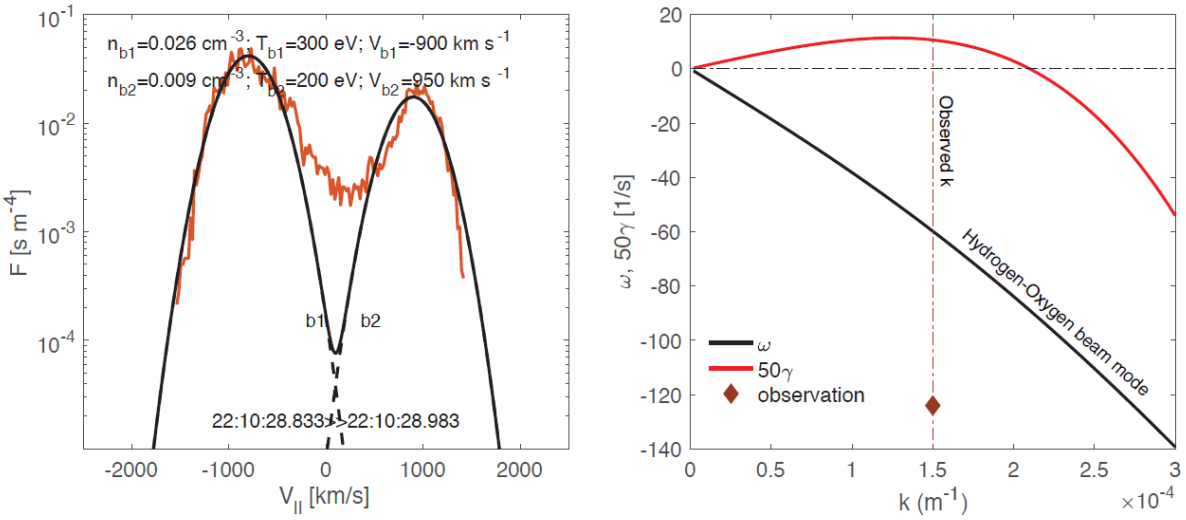

Figure 3. Instability analysis of the observed cold ion beams. (a) Maxwellian fitting of ion 1D reduced distribution. (b) predicted dispersion relation of unstable modes. The red line shows the growth rate, and the black line denotes the real frequency. The dark red diamond represents the observed wave property.

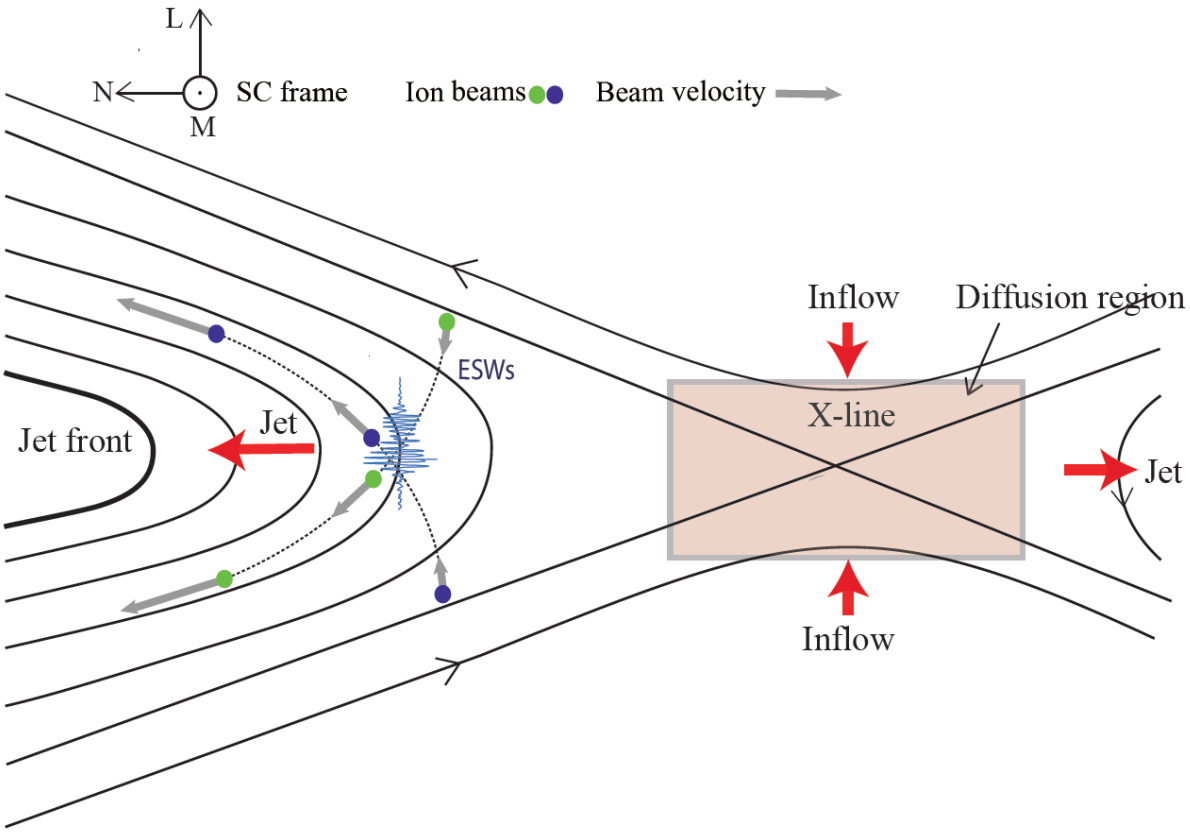

Figure 4. Sketch illustrating the formation of ion beams and the excitation of ESWs inside the reconnection jet. The ion beams are denoted by green and dark blue circles. The gray arrows represent the ion velocity in spacecraft frame, and the dashed lines represent the trajectories of the ion beams.